Flat subduction versus big mantle wedge: contrasting modes for deep hydration and overriding craton modification

Zhong-Hai Li[1]

[1]University of Chinese Academy of Sciences

November 24, 2022

Abstract

Subduction-induced deep hydration and water cycling may play significant roles in the modification and destruction of the overriding cratonic lithosphere. Two contrasting modes are generally proposed: (1) flat subduction (FS) regime with slab subducting sub-horizontally beneath the overriding lithosphere, and (2) big mantle wedge (BMW) regime with slab flattening in the mantle transition zone. Here, systematic petrological-thermomechanical models are conducted to investigate the fluid/melt activities in the contrasting subduction regimes as well as their effects on the modification of overriding lithosphere. The model results indicate that the dehydration process in the FS regime can significantly modify the overriding lithosphere for a region of about 600 km from the trench. During the progressive flat subduction, the partial melting and magmatism migrate towards the inner land of the overriding plate, which will be reversed and backward to the trench during the transition from flat to steep subduction. On the other hand, the deep hydration in the BMW regime is strongly dependent on the sub-crustal serpentinite layer in the subducting slab, whereas the oceanic crust cannot carry water to the transition zone. The modification of the overriding lithosphere in the BMW regime occurs in a larger region of >1000 km from trench, which is however generally slower and weaker. The modification and destruction of North China Craton is more likely to be controlled by the flat subduction of paleo-Pacific plate in the late Jurassic to early Cretaceous, which may be accompanied by the effects of deep water cycling in the BMW regime.

Flat subduction versus big mantle wedge: contrasting modes for deep hydration and overriding craton modification

Zhong-Hai Li [1]

[1] Key Laboratory of Computational Geodynamics, College of Earth and Planetary Sciences, University of Chinese Academy of Sciences, Beijing, China

Corresponding: Z.-H. Li (li.zhonghai@ucas.ac.cn)

Highlights:

(1) Flat slab subduction can significantly hydrate and modify the overriding cratonic lithosphere for a region of about 600 km from the trench.

(2) Sub-crustal serpentinite layer in the subducting slab controls deep water cycling and overriding plate modification in the big mantle wedge.

(3) The destruction of North China Craton is more likely to be controlled by the flat subduction of paleo-Pacific plate in the Mesozoic.

Abstract

Subduction-induced deep hydration and water cycling may play significant roles in the modification and destruction of the overriding cratonic lithosphere. Two contrasting modes are generally proposed: (1) flat subduction (FS) regime with slab subducting sub-horizontally beneath the overriding lithosphere, and (2) big mantle wedge (BMW) regime with slab flattening in the mantle transition zone. Here, systematic petrological-thermomechanical models are conducted to investigate the fluid/melt activities in the contrasting subduction regimes as well as their effects on the modification of overriding lithosphere. The model results indicate that the dehydration process in the FS regime can significantly modify the overriding lithosphere for a region of about 600 km from the trench. During the progressive flat subduction, the partial melting and magmatism migrate towards the inner land of the overriding plate, which will be reversed and backward to the trench during the transition from flat to steep subduction. On the other hand, the deep hydration in the BMW regime is strongly dependent on the sub-crustal serpentinite layer in the subducting slab, whereas the oceanic crust cannot carry water to the transition zone. The modification of the overriding lithosphere in the BMW regime occurs in a larger region of >1000 km from trench, which is however generally slower and weaker. The modification and destruction of North China Craton is more likely to be controlled by the flat subduction of paleo-Pacific plate in the late Jurassic to early Cretaceous, which may be accompanied by the effects of deep water cycling in the BMW regime.

1. Introduction

Water transportation from the surface to Earth's deep interior and its circulation in the mantle is crucial for better understanding the evolution of the planet (e.g., *Faccenda, 2014; Magni et al., 2014; Nakagawa and Nakakuki, 2019*). There are several ways for the water transportation upward, e.g., through mid-ocean ridge, mantle plume, and island arc; however, the subducting slab is the only path to transport water downward to the mantle. The subduction-induced water cycling is critical to various subduction-zone phenomena, for example, the widely studied arc magmatism (*Schmidt and Poli, 1998*) and intraslab earthquakes (*Yamasaki & Seno, 2003*), as well as the plausible overriding craton modification/destruction (*Zhu et al., 2012*).

Two subduction modes are generally proposed (*Wu et al., 2019; Zhu et al., 2019*), i.e. flat subduction and big mantle wedge (Figure 1), which may result in contrasting deep hydration processes and thus play different roles in the overriding lithospheric modification. The 'flat subduction' model indicates slab subducting sub-horizontally beneath the overriding cratonic lithosphere, like the present-day flat slab beneath Peru and central Chile (*Espurt et al., 2008*). In this regime, the flat subducting slab carries and liberates water beneath the overriding lithosphere, which may lead to hydration and weakening of the cratonic root and further contribute to its modification (Figure 1a). In addition, the mechanical bottom erosion of the overriding lithosphere by flat slab may also play a certain role (*Axen et al., 2018*). On the other hand, the 'big mantle wedge' model concerns the subducted and flatly stagnant slab in the mantle transition zone (MTZ). A certain amount of water may be carried by the sinking slab to the MTZ, which would liberate later after the slab being heated by the surrounding hot mantle. The upward migration of the water and its further interaction with the overriding lithosphere may lead to the craton modification. The key to compare and distinguish these two models is to constrain the subduction-induced deep hydration processes in the whole upper mantle, which is however far from better understanding.

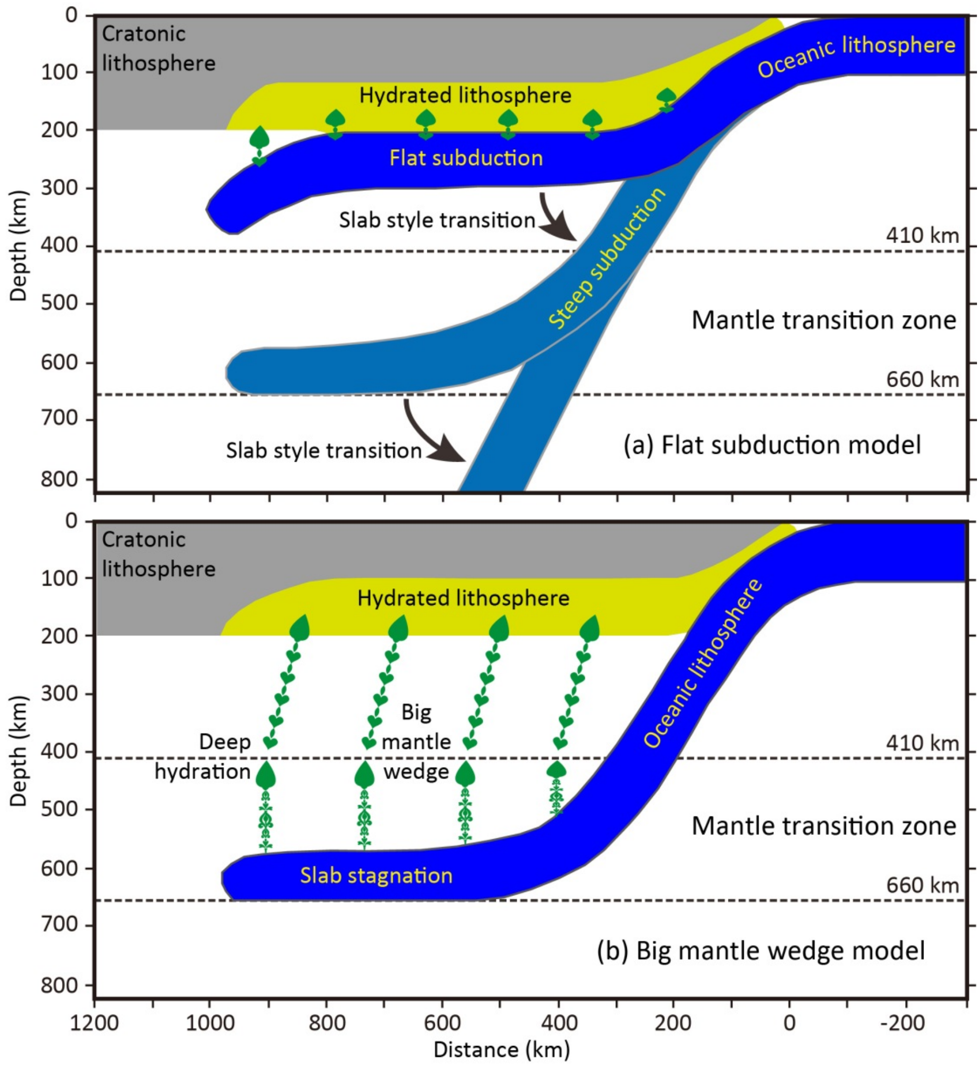

Figure 1. Two contrasting models of subduction-induced deep hydration and overriding craton modification. (a) Flat subduction model. (b) Big mantle wedge model.

It is generally accepted that the oceanic crust can contain a certain amount of water, which could be carried into the mantle by subduction and then liberate into the mantle wedge during the heating of sinking slab. However, the oceanic crust can only carry water to shallower depth (*Maruyama and Okamoto, 2007*), which thus prevent the deep hydration processes in the MTZ (*Nakao et al., 2016; Li et al., 2019*). Alternatively, the mantle serpentinites within the subducting slab could remain colder and thus carry water to greater depths than crustal rocks, which therefore may significantly contribute to the water flux at intermediate and deep depths (e.g., *Rüpke* *et al., 2004; Hacker, 2008; Van Keken et al., 2011*). The topmost lithospheric mantle of oceanic plate could be hydrated during its evolution through time (*Deschamps et al., 2013; Evans et al., 2013*), which may occur (i) along the mid-ocean ridge, where the hot mantle and extracted magma are exposed to seawater (*Sauter et al., 2013*); (ii) around the scarps and transform fault, where the seawater may penetrate downward to the sub-crustal depth (*Bideau et al., 1991; Morishita et al., 2009*); and (iii) in the outer-rise region near the trench, where seawater may flow through the outer-rise faults into the oceanic crust and underlying lithospheric mantle (*Ranero et al., 2003; Faccenda et al., 2009; Key et al., 2012*). The properties of sub-crustal hydrous layer of oceanic lithosphere are widely investigated with multiple geophysical observations (Table 1). The results indicate that the thickness (H_{serp}) and water content (W_{serp}) of this hydrous mantle layer are quite variable among different subduction zones in nature, i.e. $H_{serp} \in (0, 30)$ km and $W_{serp} \in (0, 4)$ wt% as compiled in Table 1.

Table 1. Geophysical observations of the subducting slab hydration in nature.

Subduction-zone (Segment)	Slab age (Ma)	Crustal thickness (km)	H_{serp}[a] (km)	W_{serp}[b] (wt%)	Reference
Cocos (Nicaragua)	14-24	5-20	14	<3.9	*Ranero et al., 2003*
Cocos (Nicaragua)	-	5-6.5	3-4	<3	*Ivandic et al., 2010*
Cocos (Nicaragua)	24	6	7-14	3.5	*van Avendonk et al., 2011*
Cocos (Nicaragua)	27	-	10	1.2	*Lefeldt et al., 2012*
Cocos (Costa Rica)	21.5	10	~3	1-2	*van Avendonk et al., 2011*
Nazca (N. Chile)	44	-	20	2.5	*Ranero and Sallares, 2004*
Alaska	50-55	-	3-4	1.8	*Shillington et al., 2015*
Tonga	80	7-20	<30	<3.9	*Contreras-Reyes et al., 2011*
Kuril	130	-	-	2.6	*Fujie et al., 2013*
N. & W. Pacific	100±50	-	5-15	0.5-2	*Emry and Wiens, 2015*
Mariana	150	6.5±1.5	24±5	2	*Cai et al., 2018*

(a) H_{serp} defines the thickness of hydrated lithospheric mantle layer in the subducting slab.
(b) W_{serp} is the estimated water content of the hydrated mantle layer.

In this study, we do not aim to clarify the formation mechanism of this hydrous mantle layer, but instead investigate its controls on the deep water cycling in the subduction zone as well as the contributions to the overriding craton modification.

Systematic thermomechanical models are conducted with thermodynamic fluid-melt activity, which are thus suitable for investigating both the subduction dynamics and the correlated deep hydration and water cycling.

2. Numerical model setup

The numerical models are conducted with the code I2VIS (*Gerya*, *2010*), with integrating the deep water activity down to 30 GPa in the deep mantle (*Li et al., 2019*). The detailed numerical methods and implementations are shown in the supporting information.

Large-scale models are configured in a Cartesian box of 5000 × 1400 km (Figure 2). The initial model mainly comprises two domains: an oceanic plate on the left and a continental plate on the right, with an initial weak zone in between. The oceanic lithosphere is composed of an upper crustal layer (3 km), a lower crustal layer (5 km) and a mantle layer with the thickness dependent on the age of the lithosphere (60 Ma). In addition, a sub-crustal serpentinite layer with variable thickness (0~25 km) is applied for the oceanic lithosphere. The initial thermal structure of oceanic lithosphere is defined by the half-space cooling model (e.g., *Turcotte and Schubert*, *2002*). The continental lithosphere is set up by an upper crust (20 km), a lower crust (15 km) and a mantle layer (100 km or 150 km). The initial thermal structure of continental lithosphere is laterally uniform with a linear gradient defined by 0°C at the surface and 1350°C at the bottom of lithosphere. The initial thermal gradient in the sub-lithospheric mantle is about 0.5 °C/km. On the top of the model domain, a 'sticky air' layer with low density and viscosity is applied (*Schmeling et al., 2008; Crameri et al.*, 2012), which allows the direct calculation of topography evolution, i.e. the spontaneous deformation of crustal surface. Detailed numerical parameters are shown in the supporting information (Tables S1 and S2).

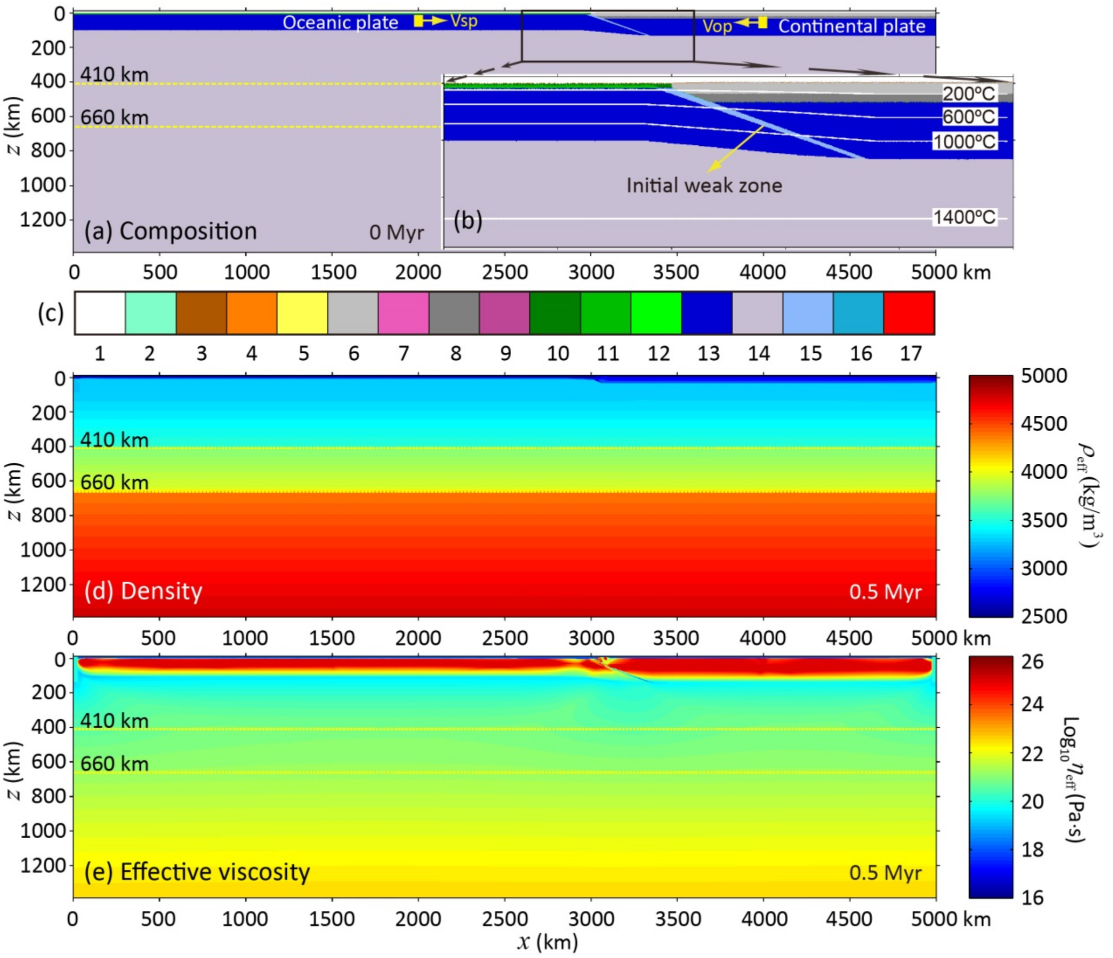

Figure 2. Initial model setup. (a) Composition field in the framework of 5000 × 1400 km, in which the 410 km and 660 km discontinuities are shown with yellow dashed lines. (b) The enlargement of initial subduction zone, with white lines showing the isotherms, starting from 200°C with the interval of 400°C. The colors in (a) and (b) indicate for rock types as specified by the colorbar in (c): 1-sticky air; 2-water; 3,4-sediment; 5-partially molten sediment; 6-continental upper crust; 7-partially molten continental upper crust; 8-continental lower crust; 9-partially molten continental lower crust; 10,11-oceanic upper and lower crust, respectively; 12-partially molten oceanic crust; 13,14-lithospheric and subjacent mantle, respectively; 15,16-hydrated and serpentinized mantle, respectively; 17-partially molten mantle. (d-e) The density and effective viscosity structures of the model domain, which are validated in *Li et al.*, (2019).

For the velocity boundary conditions, free slip is satisfied for all boundaries. The convergence velocity is applied for subduction initiation, and will be canceled after 20 Myrs, leaving the subduction driven purely by the internal buoyancy. For the thermal boundary condition, fixed values of 0ºC and 1975ºC are applied for the top and bottom boundaries, respectively. The horizontal heat flux across the vertical boundaries is zero.

The current model includes most critical processes of hydration, partial melting, and multiple phase transitions (*Li et al., 2019*). There are still some uncertainties and limitations. One uncertainty of the deep hydration model is the water capacity of nominally anhydrous minerals (NAMs) of the mantle, which is not included in the thermodynamic database (Figure S1) and is not well constrained by the laboratory experiments. The high-pressure experimental studies have shown that the water capacity in upper- and lower-mantle NAMs is generally less than 0.1~0.2wt%, whereas the NAMs in the transition zone may contain more water, e.g., on the order of 1.0wt%, or even as much as 3.0wt% (*Bolfan-Casanova et al., 2000; Murakami et al., 2002; Bercovici and Karato, 2003*). The upwelling of a hydrous MTZ may lead to magmatism in the overriding plate, which is numerically studied recently (Chen and Faccenda, 2019; Yang and Faccenda, 2020). In order for simplicity, a reference value of 0.1wt% is applied for the water capacity of the mantle NAMs, the effect of which is further tested with additional models. Another limitation lies in the partial melting of mantle rocks, which is only applied for the depths of <300 km, according to the parameterization of *Katz et al.* (2003). Thereby, the partial melting of mantle rocks is neglected in the depths of ≥300 km. It thus prevents the test of partial melting or the water filter model of the MTZ (*Bercovici and Karato, 2003*), which require further studies.

3. Model results

3.1. General model without initial serpentinite layer in the oceanic plate

In the general model setup (Figure 2), the initial water is only present in the oceanic crust which is constrained by the thermodynamic database (Figure S1), whereas the lithospheric mantle is absent of water (Figure 3a').

The converging plates are initially pushed with a constant velocity of 6 cm/yr (Figure 3e), which includes a subducting plate velocity (Vsp = 4 cm/yr) and an overriding plate velocity (Vop = -2 cm/yr). The prescribed velocities are cancelled after 20 Myrs, during which the oceanic slab subducts and stagnates in the MTZ due to the resistance of the 660-km discontinuity (Figure 3b). Afterward, the free subduction accompanied with trench retreat leads to slab flattening in the MTZ for >1000 km (Figure 3c). Finally, the steep subduction with negligible trench retreat results in slab penetration into the lower mantle (Figure 3d). During the whole subduction processes, most water of the sinking slab is lost in the sub-arc depth, whereas a certain amount of water is carried up to 250 km (Figure 3b'-d'). However, the water taken to the MTZ is very limited (≤0.1wt% in the present study), which is controlled by the prescribed water capacity of mantle NAMs (i.e. 0.1wt%).

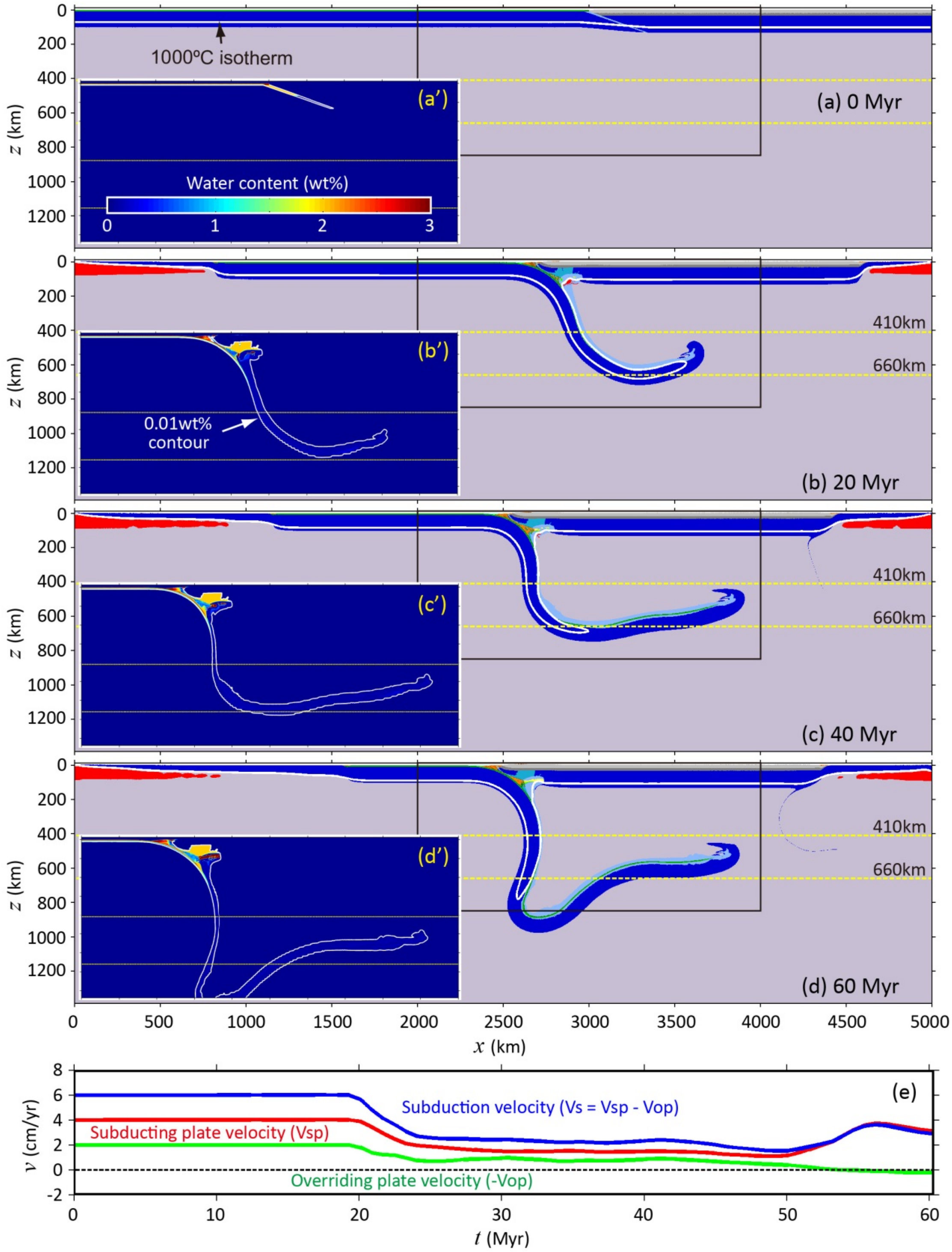

Figure 3. The general model evolution with initial water only present in the oceanic crust. (a-d) Composition field evolution with colors for rock types as specified in Figure 2c. The yellow dashed lines represent the 410 km and 660 km discontinuities, respectively. The white solid line denotes the isotherm of 1000 °C. (a'-d') Water content evolution with colorbar shown in (a'). The white line denotes the constant water content of 0.01wt%. (e) The kinematic evolutions of the converging plates, with

the red line for subducting plate velocity (Vsp), the green line for overriding plate velocity (-Vop) and the blue line for the whole subduction velocity (Vs = Vsp - Vop). The initial convergence velocity is 6 cm/yr, with Vsp = 4 cm/yr and Vop = -2 cm/yr, which are cancelled after 20 Myrs.

3.2. Reference model with an initial serpentinite layer of 20 km thick

In this model, an initial serpentinite layer is prescribed beneath the oceanic crust, which is rheologically weak and has a unified thickness of 20 km (Figure 4). All the other parameters are identical to the general model (Figure 3).

At the initial stage, the oceanic slab is sub-horizontally subducted beneath the overriding continental lithosphere (Figure 4a). The water is carried by the slab to the inner continent within about 600 km from the trench, during which a certain amount of water is liberated and migrates upwards to hydrate the continental lithosphere (Figure 4a'). The flat subduction region is characterized by cold thermal condition (Figure 4a), which thus prevents the partial melting of hydrous mantle rocks above the flatly subducting slab. The partially molten rocks (red color) are only predicted in the leading end of the flat subduction region, which has relatively high temperature due to the contact with hot asthenosphere (Figure 4a). The increasing of slab pull leads to gradual transition from flat to steep subduction (Figure 4b). The previously hydrated mantle rocks above the flat slab will be heated by the incoming asthenospheric flow, which results in the lateral migration of partial melting towards the trench (Figure 4a-c). On the other hand, a large amount of water is carried by the sinking slab, mainly by the sub-crustal hydrated mantle rocks, to the MTZ (Figure 4b'). After 20 Myrs, the prescribed convergence velocity of 6 cm/yr is canceled (Figure 4e). Then the slab subducts freely under its own negative buoyancy.

The continued subduction with trench retreat (Figure 4e) results in the formation of a big mantle wedge with the length scale of >1000 kilometers (Figure 4c). The stagnant and flatten slab at the bottom of MTZ is gradually heated by the surrounding hot mantle, which is shown by the evolution of isothermal contours (Figure 4c-d). The increasing temperature of the slab leads to the decomposition of high pressure hydro-silicates. The liberated water migrates upwards, hydrates the upper mantle as well as the overriding lithosphere (Figure 4c'-d'). The hydration process leads to the vigorous partial melting at the bottom of the continental lithosphere (Figure 4d, d').

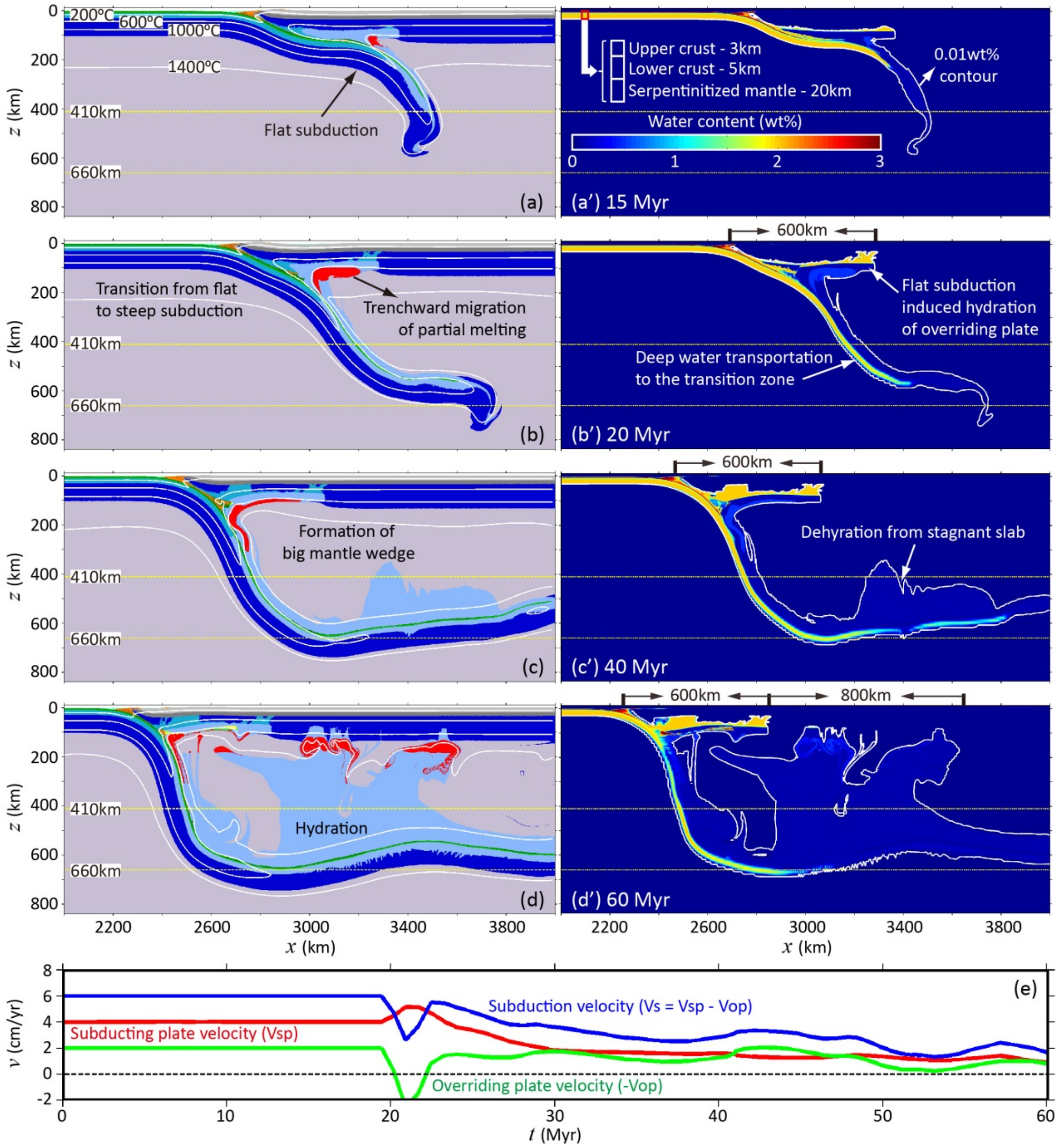

Figure 4. The model evolution with an initial serpentinite layer of 20 km thick beneath the oceanic crust. All the other parameters are identical to the general model in Figure 3. (a-d) Composition field evolution with colors for rock types as specified in Figure 2c. The yellow dashed lines represent the 410 km and 660 km discontinuities, respectively. The white solid lines denote the isotherms, starting from 200 °C with the interval of 400 °C. (a'-d') The water content evolution with initial configuration of hydrated layers in the oceanic plate as shown in (a'). The white line

denotes the constant water content of 0.01wt%. (e) The kinematic evolutions of the converging plates, with the same definitions as in Figure 3e.

The complex processes of melt extraction and further emplacement of magmatic rocks are not well constrained, which are thus not directly simulated in the current study. In order to give implications for the potential magmatic activity, the spatiotemporal distributions of partial melting are plotted (Figure 5a-b). It shows that the partial melting migrates far away from the trench during the progressive flat slab subduction, which goes instead towards the trench during the transition from flat to steep subduction, i.e. flat slab rollback. At the late stages, the partial melting occurs at the bottom of the overriding lithosphere, due to the hydration in the big mantle wedge regime, which can locate far from the trench, i.e. >1000 km.

The overriding continental lithosphere is significantly modified by the fluid and melt activities from both the flat subduction and big mantle wedge regimes (Figure 5c-d). The flat subduction can affect the regions of about 600 km from the trench, where the cratonic lithosphere is significantly modified. The thickness of unmodified lithospheric mantle is changing from the original 100 km to 0-35 km after 60 Myrs (Figure 5c), with the thickness of the whole lithosphere from 135 km to 35-70 km (Figure 5d). The flattened slab in the MTZ, i.e. the big mantle wedge regime, can affect larger regions of >1000 km from the trench; however, the degree of hydration and related cratonic modification is lower (Figure 5c-d).

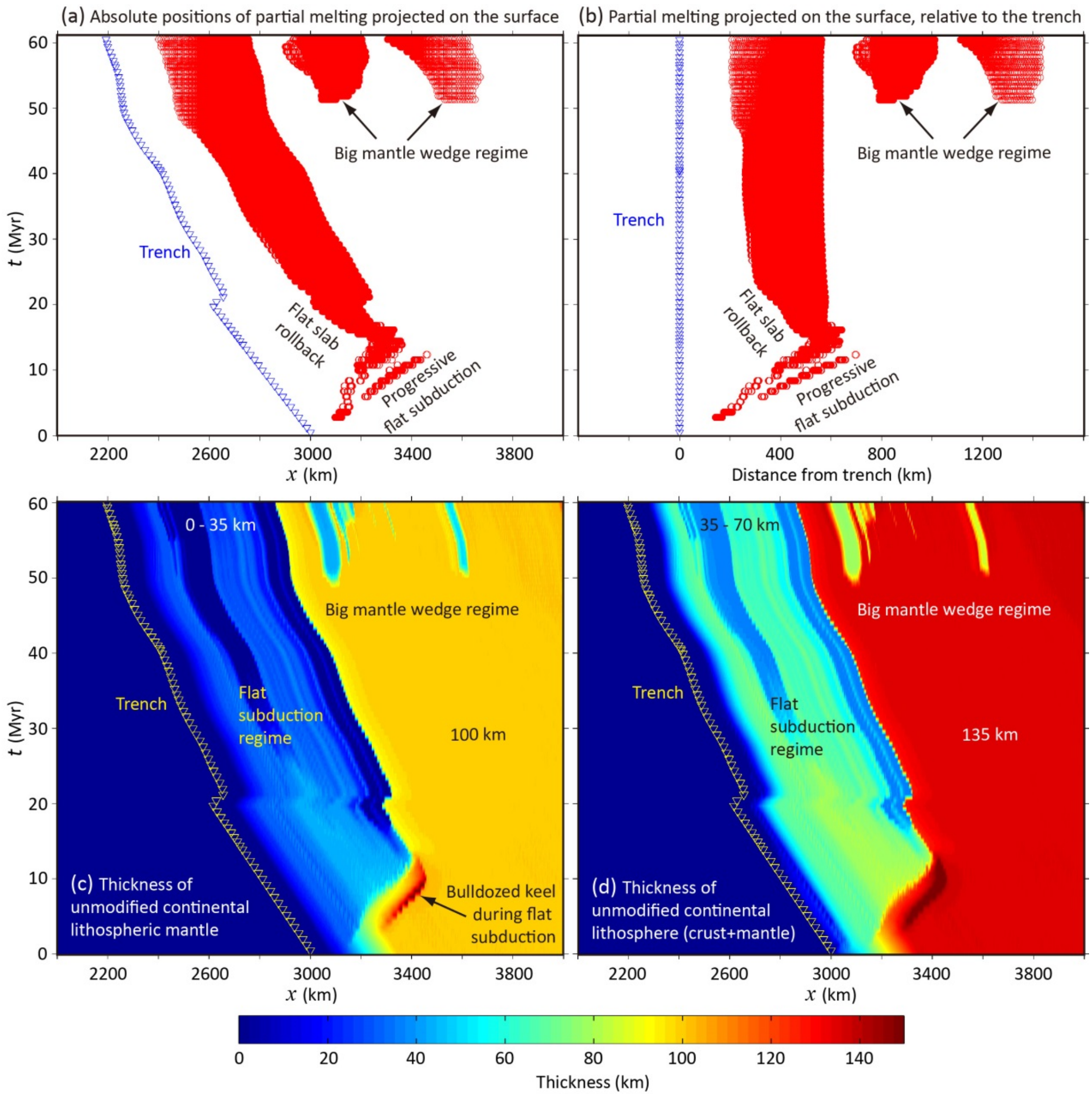

Figure 5. (a-b) The spatiotemporal distribution of partial melting during subduction-induced deep hydration. (a) Absolute positions of partial melting projected on the surface (red circles) with time-dependent trench positions (blue triangles). (b) Relative positions of partial melting projected on the surface (red circles), calculated with the distance from the trench at each time-step. (c-d) The thickness evolution of the unmodified (i.e. not hydrated) overriding continental lithospheric mantle (c) and the whole lithosphere including continental crust (d).

3.3. Effect of the thickness of initial serpentinite layer

The thickness of serpentinized mantle in the subducting slab is changing among different subduction zones in nature (Table 1), the effects of which are studied in this section (Figure 6). The model results indicate that flat subduction is not predicted if the serpentinite layer is thin, e.g., H_{serp} = 5 km (Figure 6a, a') or H_{serp} = 10 km (Figure 6b, b'). The steeply subducting slab flattens in the MTZ, with forming a big mantle wedge. The amount of water carried by the subducting slab to the MTZ is limited, which only affects the neighboring regions of the stagnant slab, but does not contribute to the modification of overriding continental lithosphere (Figure 6a, b).

In contrast, if the initial serpentinite layer is thicker, e.g., H_{serp} = 15 km or 25 km (Figure 6c-d), the subduction evolution is similar to the reference model with H_{serp} = 20 km (Figure 4). Flat subduction is formed at the initial stage, which gradually changes to the steep subduction due to the increasing of slab pull. Then the slab stagnates and flattens in the MTZ with forming a big mantle wedge. A large amount of water is carried by the slab to the MTZ, which liberates later and significantly contributes to the hydration of upper mantle and the modification of overriding continental lithosphere (Figure 6c, d).

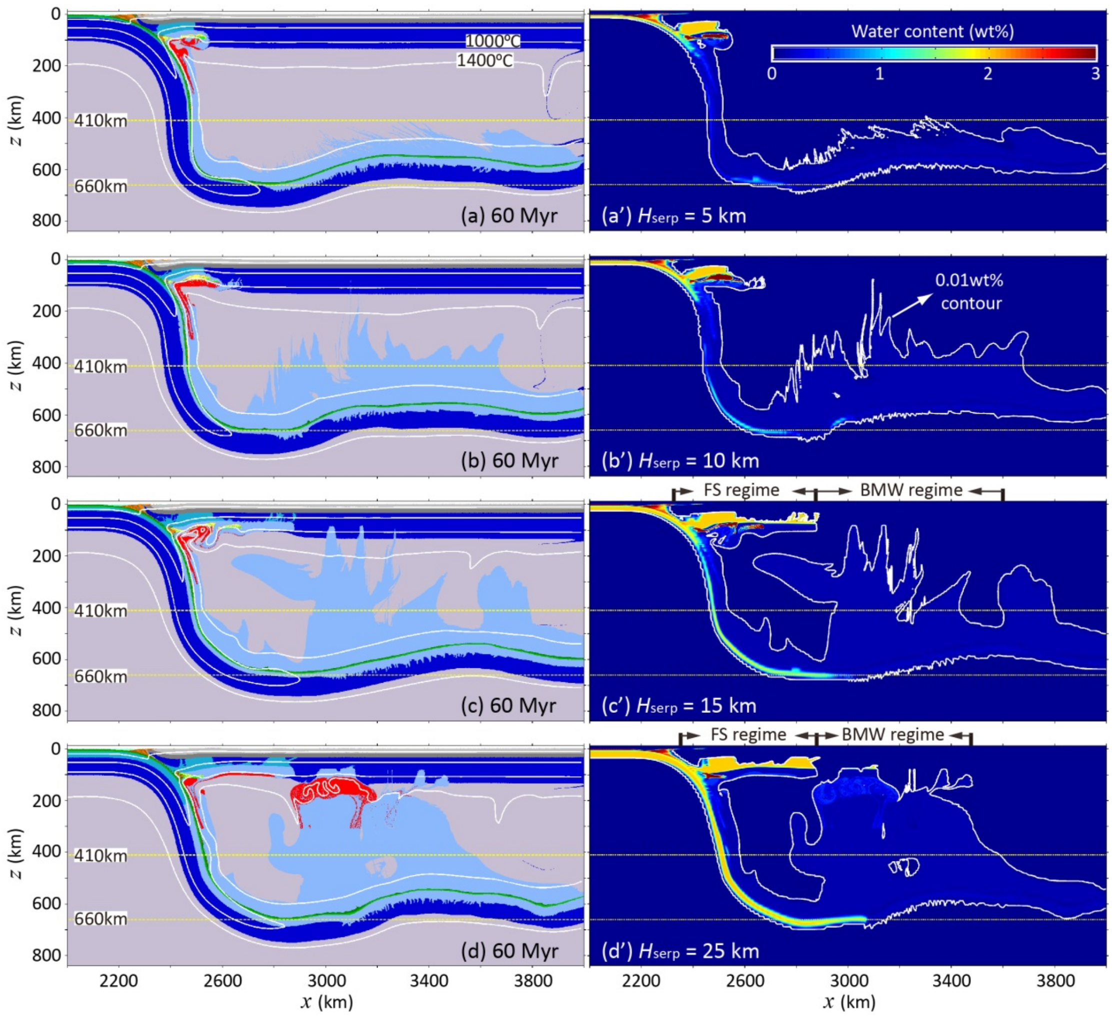

Figure 6. The model results with variable thickness of the serpentinite layer beneath the subducting oceanic crust, i.e. 5 km in (a-a'), 10 km in (b-b'), 15 km in (c-c') and 25 km in (d-d'). (a-d) Composition field evolution with colors for rock types as specified in Figure 2c. The yellow dashed lines represent the 410 km and 660 km discontinuities, respectively. The white solid lines denote the isotherms, starting from 200 °C with the interval of 400 °C. (a'-d') The water content evolution with colorbar shown in (a'). The white line denotes the constant water content of 0.01wt%.

The subduction-induced hydration and modification of overriding lithosphere is further compared in Figure 7. In the models with thinner initial serpentinite layer, the overriding lithospheric modification is restricted to a narrower region of 200-300 km with H_{serp} = 5 km (Figure 7a) and 300-400 km with H_{serp} = 10 km (Figure 7b). In contrast, a wider region of about 600 km in the overriding lithosphere is modified by flat subduction-induced hydration in the models with thicker initial serpentinite layer (Figure 7c-d). In addition, the hydration in the big mantle wedge regime may lead to an additional overriding lithospheric modification of about 600 km (e.g., Figure 7d).

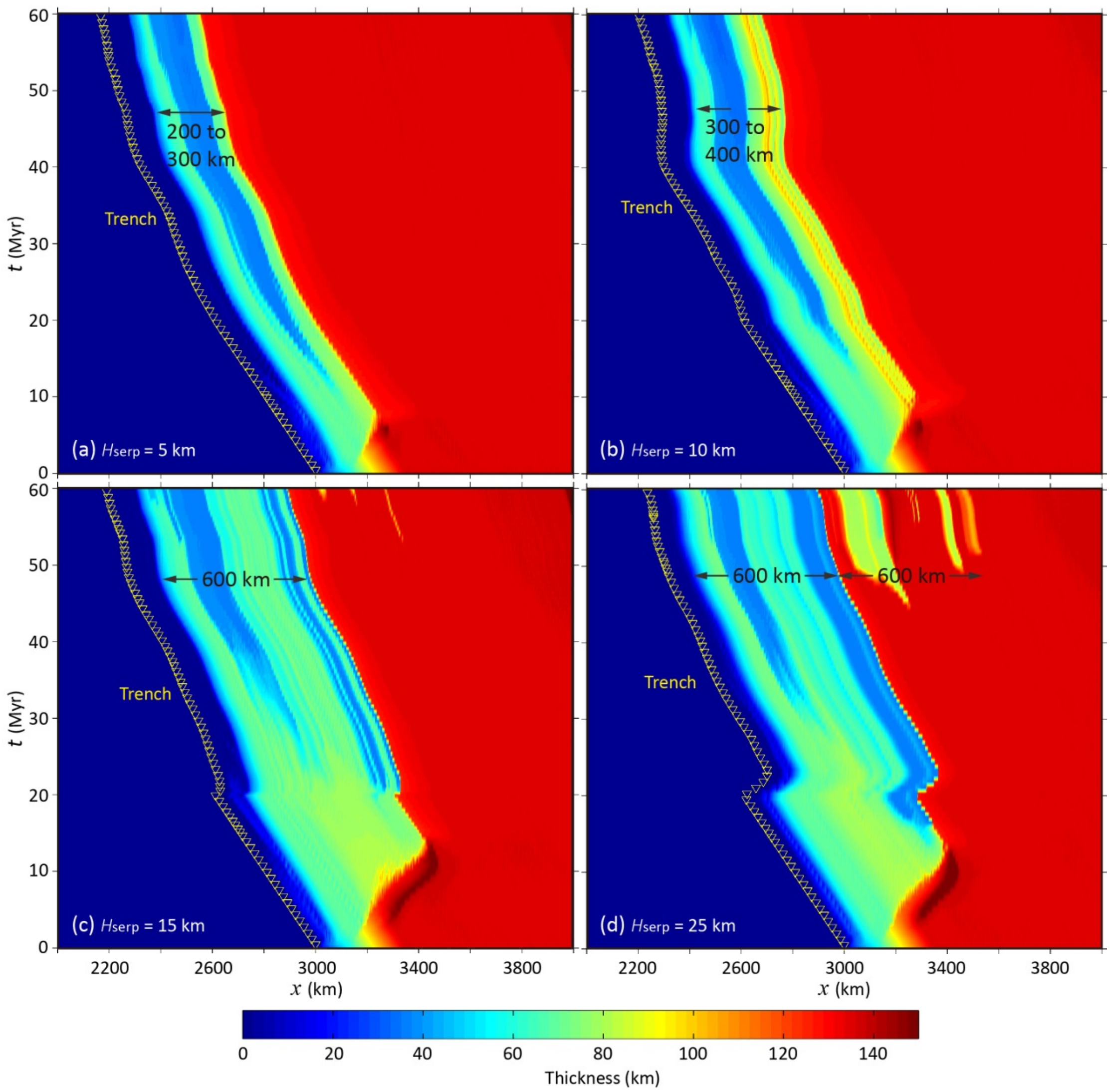

Figure 7. The thickness evolution of the unmodified (i.e. not hydrated) overriding continental lithosphere in the models with variable thickness of the serpentinite layer beneath the subducting oceanic crust, i.e. 5 km in (a), 10 km in (b), 15 km in (c) and 25 km in (d).

The formation mechanism of flat subduction is an important issue, although not the focus of this study, which has been systematically investigated previously (e.g., van Hunen et al., 2004; Huangfu et al., 2016; Manea et al., 2017). It could be attributed to many factors, for example, the young subducting slab, the oceanic plateau subduction, as well as the seaward movement of overriding plate. In this study, the complex density variation during mantle hydration is not applied, which indicates the same reference density for the dry and hydrated mantle rocks, although the density will be decreased during partial melting (Table S2). The model results show that the thick serpentinite layer contributes to the formation of flat subduction at the initial stages (c.f. Figures 3, 4 and 6), which may be due to the hydration-induced rheological weakening of the slab. Thus, the slab unbending occurs more easily when subducting to the sub-lithospheric depth, which finally results in the flat slab subduction beneath the overriding lithosphere.

3.4. Effect of a thick overriding continental lithosphere

In the previous models, the overriding continental lithosphere has a normal thickness of 135 km, which may be thinner than the stable craton (*Sleep, 2005; Peslier et al., 2010*). In this section, an additional model with a thick overriding plate of 185 km is further conducted (Figure 8). All the other parameters are identical to the reference model (Figure 4).

The general model evolution with a thick overriding plate is similar to the reference model (c.f. Figures 8 and 4). The flat slab subduction is resulting at the initial stages, which changes to steep subduction style and forms a big mantle wedge. The dehydration occurs during either the flat subduction or the slab stagnation in the MTZ. The length scale of flat subduction is similarly around 600 km from the trench, with intense hydration and modification of the overriding lithosphere (Figure 8d, d'). In contrast, the dehydration from stagnant slab in the MTZ may influence a further region from the trench, although the effects are much weaker (Figure 8d, d').

The different phenomenon in this model with a thick overriding lithosphere is the limited partial melting in either the flat subduction or big mantle wedge regimes (c.f. Figures 8 and 4). This is due to the increased solidus temperature according to the larger pressure at the bottom of the thick overriding lithosphere. Thus, the conditions of partial melting are more difficult to be achieved with the similar degree of hydration. The partial melting in this model could be promoted by increasing the water capacity of the mantle NAMs (Figure S2 in the supporting information).

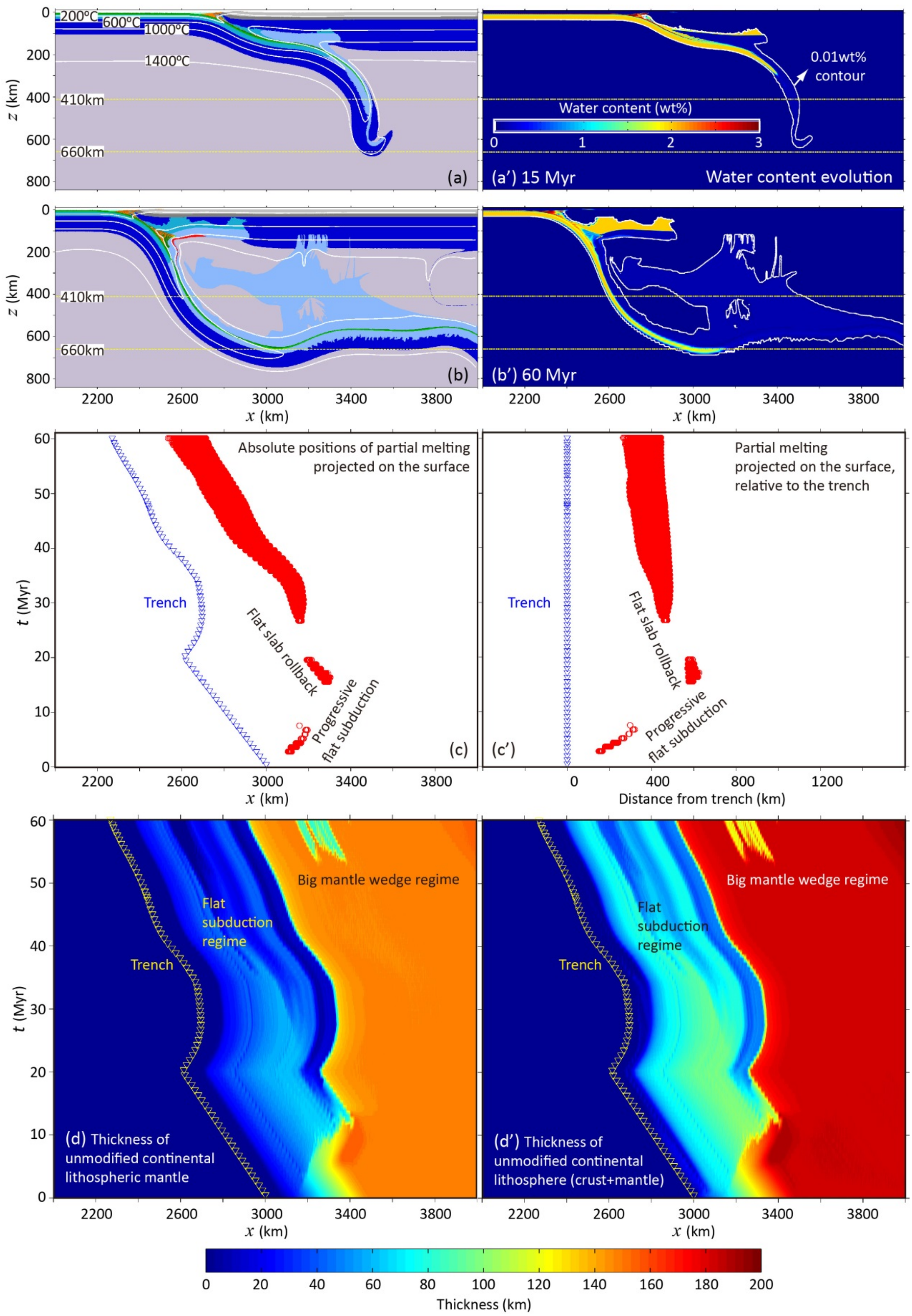

Figure 8. The model results with a thick overriding lithosphere of 185 km. All the other parameters are identical to the reference model in Figure 4 which has a normal overriding lithosphere of 135 km. (a-b) Composition field evolution with colors for rock types as specified in Figure 2c. The yellow dashed lines represent the 410 km

and 660 km discontinuities, respectively. The white solid lines denote the isotherms, starting from 200 °C with the interval of 400 °C. (a'-b') The water content evolution with colorbar shown in (a'). The white line denotes the constant water content of 0.01wt%. (c, c') The absolute and relative positions of partial melting projected on the surface (red circles) with trench positions (blue triangles). (d, d') The thickness evolution of the unmodified (i.e. not hydrated) overriding continental lithosphere.

3.5. Effect of a high water capacity (1.0wt%) of NAMs in the MTZ

The NAMs in the transition zone, i.e. primarily wadsleyite and ringwoodite, may contain more water on the order of 1.0-3.0wt% (e.g., Bercovici *and Karato, 2003*). Its effect is tested with an additional model (Figure 9), in which a high water capacity of 1.0wt% is applied for the mantle NAMs in the MTZ. The model result shows that the water released from the slab in the MTZ is totally absorbed by the neighboring mantle rocks which have a high water capacity. Thus, it differs significantly from the reference model with upward migration of hydration front (e.g., Figure 4). This model represents an end-member regime with an initially dry MTZ, which instead has a high water capacity. Not surprisingly, the limited water carried by the subducting slab can only be used to feed the 'thirsty' rocks in the MTZ. However, it is worth noting that either the pre-existing water content or the actual water capacity of the NAMs in the MTZ are not well constrained in the natural Earth. Thus, the initial water content and special water capacity of the MTZ rocks are not considered in the reference models.

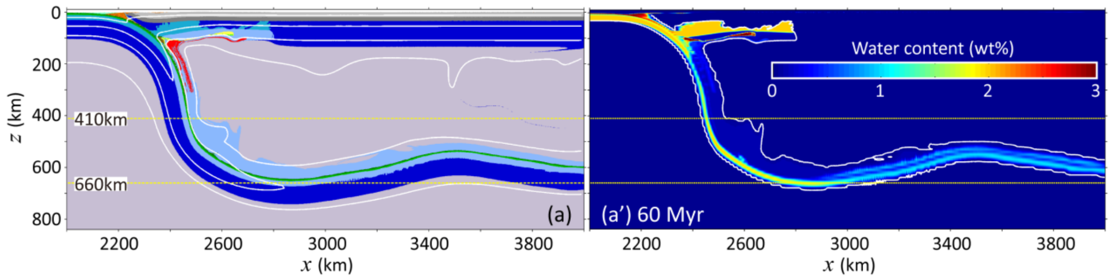

Figure 9. The model result with a high water capacity (1.0wt%) of NAMs in the MTZ. All the other parameters are identical to the reference model in Figure 4. (a) Composition field with colors for rock types as specified in Figure 2c. The yellow dashed lines represent the 410 km and 660 km discontinuities, respectively. The white

solid lines denote the isotherms, starting from 200 °C with the interval of 400 °C. (a') The water content with colorbar shown in (a'). The white line denotes the constant water content of 0.01wt%.

4. Discussion

4.1. Subduction-induced deep water cycling

The numerical models indicate that the water carried by the oceanic crust to the MTZ is negligible (Figure 3), which is mainly attributed to the low temperature condition of the 'choke point' in the water capacity diagrams of basalt and gabbro (Figure S1b-c). On the other hand, the oceanic crust is generally thin, i.e. 6-8 km, which can be easily heated by the thermal conduction during slab subduction. Even for an oceanic plateau with thicker crust of up to 32 km, it is still hard to carry water to the MTZ (Figure S3). It thus indicates that most of the water contained in the oceanic crust cannot pass through the 'choke point' of hydrous phase transitions at about 300 km depth (Figure S1b-c).

The sub-crustal serpentinite layer is an efficient way to carry water to the deeper mantle (e.g., Figure 4). The 'choke point' in the water capacity diagram of mantle rock locates at about 600 °C with the pressure of about 6 GPa (Figure S1d). The temperature condition (~600 °C) is higher than those of crustal rocks (~400-500 °C), whereas the pressure condition (~6 GPa) is lower than the crust (~10 GPa). Both conditions help to keep the temperature lower than the threshold value of 'choke point' of the hydrated mantle rocks. Consequently, significant amount of water can still be contained in the sub-crustal hydrous layer of the subducting slab and carried to the deeper mantle.

4.2. Comparisons of slab dehydration in flat subduction versus big mantle wedge regimes

The numerical models indicate that the hydration processes in both the flat subduction and big mantle wedge regimes can contribute to the overriding craton modification (e.g., Figure 4). In order to further compare their efficiencies and timescales, two simplified models are conducted (Figure 10), in which the subduction process is not simulated. In the flat subduction model, an oceanic slab (60 Ma old and 500 km long, with a 15-km-thick sub-crustal serpentinite layer is prescribed directly beneath the overriding continental lithosphere, whereas a slab with the same configuration is put at the bottom of MTZ in the big mantle wedge model.

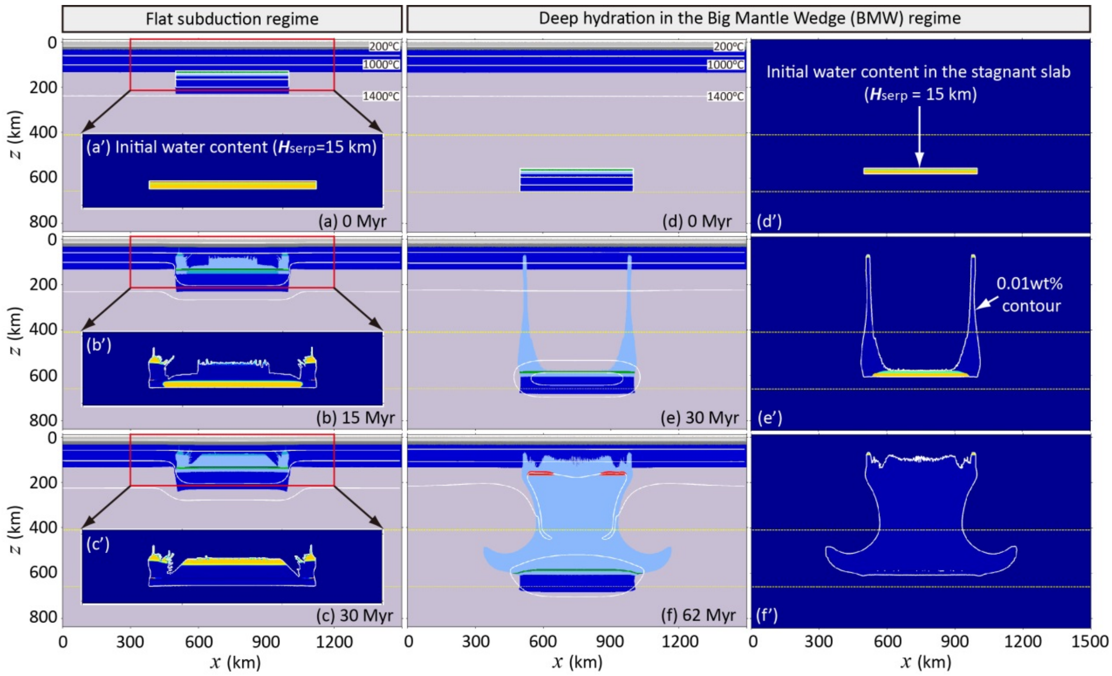

Figure 10. Comparison of water migrations in the simplified flat subduction versus big mantle wedge regimes. An initial serpentinized layer of 15 km is configured in both cases. (a-c) and (a'-c') Composition field and water content evolutions of the flat subduction regime, with an oceanic slab (60 Ma old and 500 km long) prescribed directly beneath the overriding continental lithosphere. (d-f) and (d'-f') Composition field and water content evolutions of the big mantle wedge regime, with an oceanic slab (60 Ma old and 500 km long) prescribed at the bottom of MTZ. The colors of rock types and water contents are the same as those in the above subduction models.

In both models, the dehydration occurs firstly from the edges of the oceanic slab, which then migrates to the center (Figure 10). Finally, most of water in the prescribed slab will be transported to the overriding lithosphere and upper mantle. However, the total dehydration in the flat subduction model is much faster (~30 Myrs) than that in the big mantle wedge model (~62 Myrs), because the threshold temperature condition for dehydration at a shallower depth is much lower than that with higher pressure in the MTZ (Figure S1d). Consequently, the slab dehydration in the MTZ requires high temperature condition and thus long time for heating.

Finally, the resulting hydration of overriding lithosphere is more intense in the flat subduction model than the big mantle wedge model, due to the much longer pathway of water transportation in the latter, which leads to the loss of water during the upper mantle hydration. Alternatively, most of water in the flat slab will be transferred into the cold core of the overriding lithosphere and absorbed in the hydrous minerals. Thus, the hydration-induced craton modification is more efficient in the flat subduction regime than the big mantle wedge regime, which agrees with the result of complex subduction models (e.g., Figure 4).

4.3. Implications for the modification/destruction of North China Craton (NCC)

The NCC used to have an ancient (~2.5 Ga), thick (180-200 km), and cold (~40 mW/m^2) lithosphere (e.g., *Menzies et al., 1993; Xu, 2001*); however, a present thin and hot lithosphere is observed beneath the eastern NCC (Figure 11), which suggests that the ancient cratonic root has been thinned for ~100 km. It is generally believed that the peak stage of NCC modification occurs in the early Cretaceous, or more precisely at ~125-120 Ma (*Zhu et al., 2012; Zheng et al., 2018*).

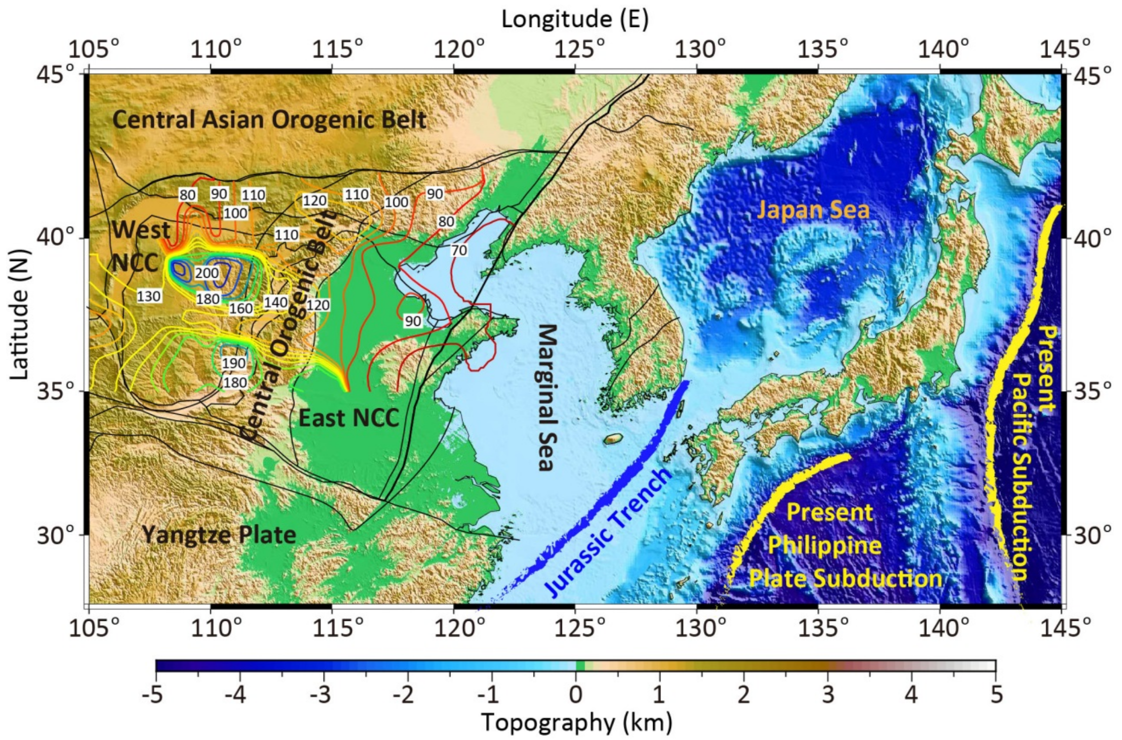

Figure 11. Tectonic background of North China Craton (NCC). Colors represent topography as shown in the colorbar at the bottom, which is produced by GMT (*Wessel et al., 2013*) with the data from ETOPO1 Global Relief Model (https://www.ngdc.noaa.gov/mgg/global/). The thin black lines are shown for the boundary faults and/or suture zones of the NCC and surrounding regions (*Zhu et al., 2012*). The thin colored lines are the contours of lithospheric thickness of NCC with the open-sourced data from 'http://www.craton.cn/data' (*Chen, 2010; Chen et al., 2014*). The thick yellow lines denote the trenches of present Pacific and Philippine plate subduction zones, respectively. The thick blue line is the estimated trench position of paleo-Pacific subduction zone in Jurassic before the major modification of eastern NCC (*Wu et al., 2019*).

It is generally accepted that the destruction of NCC is related to the fluid/melt activity during the paleo-Pacific (Izanagi) plate subduction in Mesozoic (*Liu and Li, 2018*; and references therein). The previous numerical models are generally focusing on the big mantle wedge regime. It can be further divided into two types, i.e. thermal convection (He, 2014) and hydrous MTZ upwelling (Wang et al., 2016), both of which may be followed by the bottom erosion of the overriding lithosphere. In this study, the subduction-induced hydration and overriding lithospheric modification in the flat subduction and big mantle wedge regimes are systematically compared, which are further compared to the geological records of NCC.

One of the most important geological responses of the lithospheric modification is the resulted magmatism. The most prominent magmatism in the NCC occurs in early Cretaceous, which appears to have an eastward younging trend (*Wu et al., 2019*). In contrast, the magmatism in Jurassic, i.e. before the NCC destruction, is characterized by a reverse, westward younging trend. The numerical model shows that the progressive flat subduction leads to the partial melting migrating further away from the trench (Figures 5 and 8), which is thus consistent with the westward younging trend of Jurassic magmatism in NCC. However, we need to keep in mind that it is just the potential agreement because the complex processes of magma migration as well as the further crustal-level partial melting and magmatic emplacement are not directly simulated. Afterwards, the magmatism migrates towards the trench during the transition from flat to steep subduction (Figures 5 and 8), which agrees with the eastward younging trend of early Cretaceous magmatism in NCC. On the other hand, the magmatism in the big mantle wedge regime does not show clear spatiotemporal trends, which may occur simultaneously in multiple cratonic regions above the stagnant slab (Figure 5). If constrained by the distribution of magmatism, it indicates that the flat subduction may play more important roles in the NCC modification/destruction.

A problem is the temporal and spatial scales of progressive flat subduction, which are generally short in the current numerical models, e.g., ~15 Myrs and ~600 km from the trench (e.g., Figure 4a). However, if constrained by the westward younging distribution of magmatic rocks in NCC, the progressive flat subduction may exist for the entire Jurassic of ~50 Myrs and ~2000 km from the trench (*Wu et al., 2019*). Such long flat subduction is not obtained in the current numerical models, which does also not exist in the present Earth. It is worth noting that *Wu et al.* (2019) finally estimated the flat subduction lasting for 20 Myrs, i.e. ~160-140 Ma, which is comparable to the current models (Figures 4, 8). In addition, the spatial scale of 2000 km includes the later back-arc extension and the marginal sea formation (Figure 11). If all the marginal seas are closed, backward in time to the Cretaceous, the width of east NCC is just around 600 km, which is thus consistent with not only the current numerical models, but also the maximal length of present-day flat slab beneath Peru and central Chile (*Espurt et al., 2008*).

In the big mantle wedge regime, the water liberates from the stagnant slab in the MTZ, which may further contribute to the hydration of overriding cratonic lithosphere (Figure 4). In the region close to the trench, i.e. within the flat subduction scale, the effects of both regimes are overlapped. In contrast, the region beyond the flat subduction may be purely controlled by the dehydration of stagnant slab in the MTZ, the craton modification of which is thus much weaker. The spatial scale of cratonic hydration in the big mantle wedge regime is >1000 km in the current numerical models, which is however hard to quantify and is strongly dependent on the length and thermal conditions of the stagnant slab in the MTZ. It is worth noting that the length scale of stagnant slab in the MTZ is much larger than the flatly subducted slab beneath the overriding lithosphere in both the numerical models (e.g., Figure 4) and the present-day natural Earth (*Espurt et al., 2008; Fukao and Obayashi, 2013*).

5. Conclusions

Systematic numerical models are conducted to investigate the dynamics of subduction-induced deep hydration processes and the effects on the overriding craton modification. The main conclusions from this study include the following:

(1) Subducting oceanic crust cannot carry water to the deeper mantle, i.e. the MTZ; however, the sub-crustal serpentinite layer in the sinking slab is an efficient way for the deep water cycling.

(2) Flat slab subduction can significantly hydrate the overriding cratonic lithosphere for a region within about 600 km from the trench. During the progressive flat subduction, the partial melting and magmatism migrate far away from the trench, which will be reversed and backward to the trench during the transition from flat to

steep subduction.

(3) Subduction-induced deep hydration in the MTZ and big mantle wedge is strongly dependent on the sub-crustal serpentinite layer in the sinking slab. It can contribute to the overriding craton modification for a larger region of >1000 km from the trench, which is however generally slower and weaker than the flat subduction regime.

(4) The modification/destruction of North China Craton is more likely to be controlled by the flat subduction of paleo-Pacific plate in the late Jurassic to early Cretaceous, although the slab stagnation in the MTZ, i.e. the big mantle wedge regime, may also play a certain role.

Acknowledgement

This work was supported by the NSFC projects (41688103) and the Strategic Priority Research Program (B) of CAS (XDB18000000). Numerical simulations were run with the clusters of National Supercomputer Center in Guangzhou (Tianhe-II). *T. Gerya*, *J. Connolly* and *S. Karato* are greatly acknowledged for the helpful discussion. The topographic map of Figure 11 is produced with GMT (*Wessel et al., 2013*) with the data from ETOPO1 Global Relief Model (*https://www.ngdc.noaa.gov/mgg/global/*). The contours of lithospheric thickness in Figure 11 are plotted with the open-sourced data from the Crust and Upper Mantle Velocity Model of North China v2.0 (*http://www.craton.cn/data*). The figures of numerical models are produced by Matlab and further compiled by Adobe Illustrator. All the related data will be provided in the public repository of Zenodo (https://doi.org/10.5281/zenodo.xxxxxxx).

References

Axen, G.J., Van Wijk, J.W., Currie, C.A., 2018. Basal continental mantle lithosphere displaced by flat-slab subduction. Nature Geo. 11, 961-964.

Behn, M.D., Kelemen, P.B., 2003. Relationship between seismic P-wave velocity and the composition of anhydrous igneous and meta-igneous rocks. Geochem., Geophys., Geosyst. 4(5), doi:10.1029/2002GC000393.

Bercovici, D., Karato, S.I., 2003. Whole-mantle convection and the transition-zone water filter. Nature 425, 39-44.

Bideau, D., Hebert, R., Hekinian, R., Cannat, M., 1991. Metamorphism of deep-seated rocks from the garrett ultrafast transform (East Pacific Rise Near 13o25'S). J. Geophys. Res. 96, B6, 10079-10099.

Bina, C.R., Helffrich, G., 1994. Phase transition Clapeyron slopes and transition zone seismic discontinuity topography. J. Geophys. Res. 99(B8), 15853-15860.

Bittner, D., Schmeling, H., 1995. Numerical modeling of melting processes and induced diapirism in the lower crust. Geophys. J. Int. 123, 59-70.

Bolfan-Casanova, N., Keppler, H., Rubie, D., 2000. Water partitioning between nominally anhydrous minerals in the $MgO–SiO_2–H_2O$ system up to 24GPa: implications for the distribution of water in the earth's mantle. Earth Planet. Sci. Lett. 182, 209-221.

Cai, C., Wiens, D., Shen, W., Eimer, M., 2018. Water input into the Mariana subduction zone estimated from ocean-bottom seismic data. Nature 563, 389-392.

Chen, L., 2010. Concordant structural variations from the surface to the base of the upper mantle in the North China Craton and its tectonic implications. Lithos 120, 96-115.

Chen, L., Jiang, M.M., Yang, J.H., Wei, Z.G., Liu, C.Z., Ling, Y., 2014. Presence of an intralithospheric discontinuity in the central and western North China Craton: Implications for destruction of the craton. Geology 42, 223-226.

Chen L., Faccenda M., 2019. Subduction-induced upwelling of a hydrous transition zone: Implications for the Cenozoic magmatism in Northeast China. Journal of Geophysical Research: Solid Earth, 124, 11489-11504.

Clauser, C., Huenges, E., 1995. Thermal conductivity of rocks and minerals, in: Ahrens, T.J. (ed.), Rock physics and phase relations, American Geophysical Union, Reference Shelf 3, Washington D.C., pp. 105-126.

Connolly, J.A.D., 2005. Computation of phase equilibria by linear programming: A tool for geodynamic modeling and an application to subduction zone decarbonation. Earth Planet. Sci. Lett. 236, 524-541.

Contreras-Reyes, E., Grevemeyer, I., Watts, A., Flueh, E., Peirce, C., Moeller, S., Papenberg, C., 2011. Deep seismic structure of the Tonga subduction zone: Implications for mantle hydration, tectonic erosion, and arc magmatism. J. Geophys Res. 116, B10103.

Crameri, F., Schmeling, H., Golabek, G. J., Duretz, T., Orendt, R., Buiter, S., May, D., Kaus, B., Gerya, T.V., Tackley, P., 2012. A comparison of numerical surface topography calculations in geodynamic modelling: an evaluation of the 'sticky air' method. Geophys. J. Int. 189, 38-54.

Deschamps, F., Godard, M., Guillot, S., Hattori, K., 2013. Geochemistry of subduction zone serpentinites: A review. Lithos 178, 96-127.

Dziewonski, A.M., Anderson, D.L., 1981. Preliminary reference Earth model. Phys. Earth Planet. Inter. 25, 297-356.

Emry, E., Wiens, D., 2015. Incoming plate faulting in the Northern and Western Pacific and implications for subduction zone water budgets. Earth Planet. Sci. Lett. 414, 176-186.

Espurt, N., Funiciello, F., Martinod, J., Guillaume, B., Regard, V., Faccenna, C., Brusset, S., 2008. Flat subduction dynamics and deformation of the South American plate: Insights from analog modeling. Tectonics 27, TC3011.

Evans, B., Hattori, K., Baronnet, A., 2013. Serpentinite: What, Why, Where?. Elements 9, 99-106.

Faccenda, M., Gerya, T., Burlini, L., 2009. Deep slab hydration induced by bending-related variations in tectonic pressure. Nature Geo. 790-793.

Faccenda, M., 2014. Water in the slab: A trilogy. Tectonophys. 614, 1-30.

Fujie, G., Kodaira, S., Yamashita, M., Sato, T., Takahashi, T., Takahashi, N., 2013. Systematic changes in the incoming plate structure at the Kuril trench. Geophys. Res. Lett. 40, 88-93.

Fukao, Y., Obayashi, M., 2013. Subducted slabs stagnant above, penetrating through, and trapped below the 660 km discontinuity. J. Geophys. Res. 118, 5920-5938.

Gale, A., Dalton, C.A., Langmuir, C.H., Su, Y., Schilling, J.G., 2013. The mean composition of ocean ridge basalts. Geochem., Geophys., Geosyst. 14(3), doi:10.1029/2012GC004334.

Gerya, T.V., Connolly, J.A.D., Yuen, D.A., Gorczyk, W., Capel, A.M., 2006. Seismic implications of mantle wedge plumes. Phys. Earth Planet. Inter. 156, 59-74.

Gerya, T.V., 2010. Introduction to numerical geodynamic modelling. Cambridge University Press, Cambridge, UK.

Gorczyk W., Willner, A.P., Gerya, T., Connolly J., Burg, J.-P., 2007. Physical controls of magmatic productivity at Pacific-type convergent margins: Numerical modelling. Phys. Earth Planet. Inter. 163, 209-232.

Hacker, B.R., 2008. H_2O subduction beyond arcs. Geochem. Geophys. Geosyst. 9(3), Q03001.

Hart, S.R., Zindler, A., 1986. In search of a bulk-Earth composition. Chemical Geo. 57, 247-267.

He, L., 2014. Numerical modeling of convective erosion and peridotite-melt interaction in big mantle wedge: Implications for the destruction of the North China Craton. J. Geophys. Res.-Solid Earth 119, 3662-3677.

Huangfu, P., Wang, Y., Cawood, P., Li, Z.-H., Fan, W., Gerya, T., 2016. Thermo-mechanical controls of flat subduction: insights from numerical modeling. Gondwana Res. 40, 170-183.

Ivandic, M., Grevemeyer, I., Bialas, J., Petersen, C., 2010. Serpentinization in the trench-outer rise region offshore of Nicaragua: constraints from seismic refraction and wide-angle data. Geophys. J. Int. 180, 1253-1264.

Ito, K., Kennedy, G., 2013. An experimental study of the basalt-garnet granulite-eclogite transition, in: Heacock, J.G. (Ed.), The Structure and Physical Properties of the Earth's Crust, American Geophysical Union, Washington, DC.

Kameyama, M., Yuen, D.A., Karato, S.-I., 1999. Thermal-mechanical effects of low-temperature plasticity (the peierls mechanism) on the deformation of viscoelastic shear zone. Earth Planet. Sci. Lett. 1-2, 159-172.

Karato, S., Wu, P., 1993. Rheology of the upper mantle: A synthesis. Science 260(5109), 771-778.

Karato, S., Riedel, M., Yuen, D.A., 2001. Rheological structure and deformation of subducted slabs in the mantle transition zone: Implications for mantle circulation and deep earthquakes. Phys. Earth Planet. Inter. 127, 83-108.

Katz, R.F., Spiegelman, M., Langmuir, C.H., 2003. A new parameterisation of hydrous mantle melting. Geochem. Geophys. Geosyst. 4, 1073.

Key, K., Constable, S., Matsuno, T., Evans, R., Myer, D., 2012. Electromagnetic detection of plate hydration due to bending faults at the Middle America Trench. Earth Planet. Sci. Lett. 351-352, 45-53.

Kirby, S.H., Kronenberg, A.K., 1987. Rheology of the lithosphere: selected topics. Rev. Geophys. 25, 1219-1244.

Lefeldt, M., Ranero, C., Grevemeyer, I., 2012. Seismic evidence of tectonic control on the depth of water influx into incoming oceanic plates at subduction trenches. Geochem. Geophys. Geosyst. 13(5), Q05013.

Li, Z.H., Liu, M., Gerya, T., 2016. Lithosphere delamination in continental collisional orogens: A systematic numerical study. J. Geophys. Res. Solid Earth, 121, 5186-5211.

Li, Z.H., Gerya, T.V., Connolly, J., 2019. Variability of subducting slab morphologies in the mantle transition zone: Insight from petrological-thermomechanical modeling. Earth-Sci. Rev. 196, 102874.

Liu, M., Li, Z., 2018. Dynamics of thinning and destruction of the continental cratonic lithosphere: Numerical modeling. Sci. China Earth Sci. 61(7), 823-852.

Magni, V., Bouilhol, P., Van Hunen, J., 2014. Deep water recycling through time. Geochem. Geophys. Geosyst. 15, 4203-4216.

Manea V., Manea M., Ferrari, L., Orozco, T., Valenzuela, R., Husker, A.,Kostoglodov, V., 2017. A review of the geodynamic evolution of flat slab subduction in Mexico,Peru, and Chile. Tectonophys. 695, 27-52.

Maruyama, S., Okamoto, K., 2007. Water transportation from the subducting slab into the mantle transition zone. Gondwana Res. 11, 148-165.

Menzies, M.A., Fan, W.M., Zhang, M., 1993. Palaeozoic and Cenozoic lithoprobe and the loss of >120 km of Archean lithosphere, Sino-Korean craton, China. In: Magmatic Processes and Plate Tectonics, Prichard, H.M., Alabaster, T., Harris, N., Neary, C. (ed.), pp. 71-81, Geol. Soc. London.

Morishita, T., Hara, K., Nakamura, K., Sawaguchi, T., Tamura, A., Arai, S., Okino, K., Takai K., Kumagai, H., 2009. Igneous, alteration and exhumation processes recorded in abyssal peridotites and related fault rocks from an oceanic core complex along the central Indian ridge. J. Petro. 50(7), 1299-1325.

Nakagawa, T., Nakakuki, T., 2019. Dynamics in the Uppermost Lower Mantle: Insights into the Deep Mantle Water Cycle Based on the Numerical Modeling of Subducted Slabs and Global-Scale Mantle Dynamics. Annu. Rev. Earth Planet. Sci. 47, 41-66.

Nakao, A., Iwamori, H., Nakakuki, T., 2016. Effects of water transportation on subduction dynamics: Roles of viscosity and density reduction. Earth Planet. Sci. Lett. 454, 178-191.

Peslier, A.H., Woodland, A.B., Bell, D.R., Lazarov, M. (2010). Olivine water contents in the continental lithosphere and the longevity of cratons. Nature, 467, 78-81.

Plank, T., Langmuir, C.H., 1998. The chemical composition of subducting sediment and its consequences for the crust and mantle. Chemical Geo. 145, 325-394.

Ranalli, G., 1995. Rheology of the earth, deformation and flow process in geophysics and geodynamics (2nd ed.), Chapman & Hall, London, UK.

Ranero, C., Morgan, J., Mclntosh, K., Reichert, C., 2003. Bending-related faulting and mantle serpentinization at the Middle America trench. Nature 425, 367-373.

Ranero, C., Sallares, V., 2004. Geophysical evidence for hydration of the crust and mantle of the Nazca plate during bending at the north Chile trench. Geology 32(7), 549-552.

Rubie, D.C., Ross, C.R., 1994. Kinetics of the olivine-spinel transformation in subducting lithosphere: experimental constraints, and implications for deep slab processes. Phys. Earth Planet. Inter. 86, 223-241.

Rüpke, L.H., Morgan, J.P., Hort, M., Connolly, J.A.D., 2004. Serpentine and the subduction zone water cycle. Earth Planet. Sci. Lett. 223, 17-34.

Sauter, D., Cannat, M., Roumejon, S., Andreani, M., Birot, D., Bronner, A., Brunelli, D., Carlut, J., Delacour, A., Guyader, V., MacLeod, C., Manatschal, G., Mendel, V., Menez, B., Pasini, V., Ruellab, E., Searle, R., 2013. Continuous exhumation of mantle-derived rocks at the Southwest Indian Ridge. Nature Geo. 6, 314-320.

Schmeling, H., Babeyko, A.Y., Ennsa, A., Faccenna, C., Funiciello, F., Gerya, T., Golabek, G.J., Grigull, S., Kaus, B., Morra, G., Schmalholz, S., Van Hunen, J., 2008. A benchmark comparison of spontaneous subduction models-Towards a free surface. Phys. Earth Planet. Inter. 171, 198-223.

Schmidt M.W., Poli, S., 1998. Experimentally based water budgets for dehydrating slabs and consequences for arc magma generation. Earth Planet. Sci. Lett. 163, 361-379.

Shillington, D., Becel, A., Nedimovic, M., Kuehn, H., Webb, S., Abers, G., Keranen, K., Li, J., Delescluse, M., Mattei-Salicrup, G., 2015. Link between plate fabric, hydration and subduction zone seismicity in Alaska. Nature Geo. 8, 961-964.

Sleep, N.H., 2005. Evolution of the continental lithosphere. Annu. Rev. Earth Planet. Sci., 33, 369-393.

Turcotte, D.L., Schubert, G., 2002. Geodynamics, Cambridge University Press, Cambridge, UK.

Van Avendonk, H., Holbrook, W., Lizarralde, D., Denyer, P., 2011. Structure and serpentinization of the subducting Cocos plate offshore Nicaragua and Costa Rica. Geochem. Geophys. Geosyst. 12(6), Q06009.

Van Hunen, J., van den Berg, A.P., Vlaar, N.J., 2004. Various mechanisms to induce present-day shallow flat subduction and implications for the younger Earth: a numerical parameter study. Phys. Earth Planet. Int. 146, 179-194.

Van Keken, P., Hacker, B., Syracuse, E., Abers, G., 2011. Subduction factory: 4. Depth-dependent flux of H2O from subducting slabs worldwide. J. Geophys. Res. 116, B01401.

Wang, Z., Kusky, T.M., Capitanio, F.A., 2016. Lithosphere thinning induced by slab penetration into a hydrous mantle transition zone. Geophys. Res. Lett. 43, doi:10.1002/2016GL071186.

Wessel, P., Smith, W.H.F., Scharroo, R., Luis, J., Wobbe, F., 2013. Generic Mapping Tools: Improved Version Released. EOS Trans. AGU 94(45), 409-410, doi:10.1002/2013EO450001.

Wu, F.-Y., Yang, J.-H., Xu, Y.-G., Wilde, S.A., Walker, R.J., 2019. Destruction of the North China Craton in the Mesozoic. Annu. Rev. Earth Planet. Sci. 47, 173-95.

Xu, Y.G., 2001. Thermo-tectonic destruction of the Archean lithospheric keel beneath eastern China: evidence, timing and mechanism. Phys. Chem. Earth A 26, 747-57.

Yamasaki, T., Seno, T., 2003. Double seismic zone and dehydration embrittlement of the subducting slab. J. Geophys. Res. 108 (B4), 2212.

Yang, J., Faccenda, M., 2020. Intraplate volcanism originating from upwelling hydrous mantle transition zone. Nature, 579, 88-91.

Zheng, Y.F., Xu , Z., Zhao, Z.F., Dai, L.Q., 2018. Mesozoic mafic magmatism in North China: implications for thinning and destruction of cratonic lithosphere. Sci. China Earth Sci. 61, 353-385.

Zhu, R.X., Yang, J.H., Wu, F.Y., 2012. Timing of destruction of the North China Craton. Lithos 149, 51-60.

Zhu, R., Xu, Y., 2019. The subduction of the west Pacific plate and the destruction of the North China Craton. Sci. China Earth Sci. 62(9), 1340-1350.